Computational Materials Science 82 (2014) 310–313

Contents lists available at ScienceDirect

Computational Materials Science

journal homepage: www.elsevier.com/locate/commatsci

Role of hydrogen in the growth of boron nitride: Cubic phase versus hexagonal phase

Dong Han [a,b], Xian-Bin Li [a,*], Y.Y. Sun [b], S.B. Zhang [a,b], Sheng-Yi Xie [a], Sukit Limpijumnong [c,*], Zhan-Guo Chen [a], Hong-Bo Sun [a]

[a] State Key Laboratory on Integrated Optoelectronics, College of Electronic Science and Engineering, Jilin University, Changchun 130012, China
[b] Department of Physics, Applied Physics & Astronomy, Rensselaer Polytechnic Institute, Troy, NY 12180, USA
[c] School of Physics and NANOTEC-SUT Center of Excellence on Advanced Functional Nanomaterials, Suranaree University of Technology, Nakhon Ratchasima 30000, Thailand

ARTICLE INFO

Article history:
Received 23 March 2013
Received in revised form 27 September 2013
Accepted 30 September 2013
Available online 30 October 2013

Keywords:
Boron nitride
Hydrogen
sp^3 Nucleus
Transition from *h*BN to *c*BN
First-principles study

ABSTRACT

Hydrogen (H) behavior in crystal boron nitride (BN) has been systematically investigated by first-principles calculation. We find that H prefers to reside in the hexagonal phase (*h*BN) rather than the cubic phase (*c*BN). These kinds of H tend to gather to form clusters. In *h*BN, H can terminate a framework around an impurity-induced sp^3 nucleus, thereby suppressing the *c*BN growth. This explains why there is no significant improvement in the *h*BN-to-*c*BN transition after aluminium (Al) doping.

© 2013 Elsevier B.V. All rights reserved.

1. Introduction

The binary semiconductor boron nitride (BN) has extraordinary properties and is regarded as an important candidate for electronic, optical, and other engineering applications [1–4]. There are two frequently used BN crystals: the hexagonal BN (*h*BN) and the cubic BN (*c*BN). The *h*BN phase with a direct band gap of 6 eV holds promise for ultraviolet device applications [4]. The *c*BN phase has a wide band gap and shows high thermal conductivity and extreme hardness, which makes it suitable for high-temperature electronic devices and use as an abrasive [5–7]. To synthesize pure BN crystal, especially the high-quality *c*BN, hydrogen (H) is a common background impurity during the CVD growth process [8–11]. As a result, a significant amount of H is unavoidably present in BN, and it impacts both material quality and device performance [12].

However, the behavior of H during the growth of BN is not well understood, especially at the microscopic scale. H prefers etching the sp^2-bonding phase to the sp^3-bonding phase. This etching selectivity is the key to synthesizing high-quality diamond [13]. However, it has been argued that H exhibits no significant etching selectivity for diamond-like *c*BN or graphite-like *h*BN [14]. So the growth of high-quality *c*BN is a more challenging task. In fact, intentional doping has also been used in an attempt to promote the growth of *c*BN. So the defect physics of H on BN as well as its doped sample is a worthy topic for further exploration.

Through first-principles calculation, we proved that H is more likely to be incorporated during the growth of *h*BN rather than that of *c*BN. During *h*BN growth we were surprised to discover that the formation energy of H can be reduced by increasing its concentration. At low concentrations, H generally prefers the H_2 molecular form. However, at high concentrations, a new form of H called H_2^{**} forms—in which one H binds to B and another binds to the neighboring N. By Al doping, Al_B serves as a cubic nucleus in *h*BN. However, the presence of H prevents additional B and N from binding to the nucleus and ultimately suppresses the growth of *c*BN.

2. Calculation details

Our first-principles calculation is based on density functional theory (DFT) within local density approximation (LDA) [15]. The projector augmented-wave potentials [16] are used as implemented in the VASP code [17]. The cutoff energy for the plane-wave basis is 400 eV. We obtained the lattice parameters $a = 3.583$ Å for *c*BN, and $a = 2.492$ Å, $c/a = 2.604$ for *h*BN. Both lattice constants a are only 1% smaller than experiment, and the c is

* Corresponding author. Tel.: +86 43185168203.
E-mail addresses: lixianbin@jlu.edu.cn (X.-B. Li), sukit@sut.ac.th (S. Limpijumnong).

0927-0256/$ - see front matter © 2013 Elsevier B.V. All rights reserved.
http://dx.doi.org/10.1016/j.commatsci.2013.09.065

smaller than experiment by 3% [18]. For defect calculations, large enough supercells are employed for *c*BN (216 atoms) and for *h*BN (200 atoms). Geometry optimization with $2 \times 2 \times 2$ Monkhorst–Pack *k*-point mesh is carried out until the Hellman–Feynman force on each atom is less than 0.05 eV/Å.

3. Results and disscusion

3.1. Structural form and stability

First, we studied H in *c*BN and *h*BN; their stability can be quantitatively reflected by formation energy. Following Ref. [19], the formation energy of a defect with *n*H atoms in *c*BN or *h*BN can be defined as:

$$E^f(n\mathrm{H}) = E_{tot}(n\mathrm{H}) - E_{tot}(bulk) - n\mu(\mathrm{H}), \tag{1}$$

where $E_{tot}(n\mathrm{H})$ is the total energy of a supercell containing *n*H atoms in BN. $E_{tot}(bulk)$ is the total energy of the same supercell without defect. $\mu(\mathrm{H})$ is the chemical potential of H. Here, the growth or annealing condition defines the chemical potential for B and N. Under thermal equilibrium, the chemical potential of the host atom must satisfy $\mu(\mathrm{B}) + \mu(\mathrm{N}) = \Delta H_f(\mathrm{BN})$, where $\mu(\mathrm{B})$ and $\mu(\mathrm{N})$ are the chemical potentials of B and N, respectively, and $\Delta H_f(\mathrm{BN})$ is the formation enthalpy of BN in the cubic or hexagonal phase. The upper limit of the chemical potential is limited by its stable form under standard conditions. Here, B solid and N_2 gas are set as the limit and reference for the B/N chemical potential. So, the range of chemical potential is written as:

$$(\text{B-poor condition})\Delta H_f(\mathrm{BN}) \leqslant \mu(\mathrm{B}) \leqslant 0(\text{B-rich condition}) \tag{2}$$

$$(\text{N-poor condition})\Delta H_f(\mathrm{BN}) \leqslant \mu(\mathrm{N}) \leqslant 0(\text{N-rich condition}) \tag{3}$$

Usually, the upper limit of the H chemical potential, $\mu(\mathrm{H})$, is defined by H_2 gas. Here, in the presence of N, we should also consider a secondary product (i.e., NH_3) during the growth. So, the chemical potential of H is defined as:

$$\mu(\mathrm{H}) \leqslant \frac{\Delta_f H(\mathrm{NH_3}) - \mu(\mathrm{N})}{3} \quad \text{and} \quad \mu(\mathrm{H}) \leqslant 0 \tag{4}$$

In Fig. 1(a), the formation energies of the H interstitial, H_2, and H complexes (labeled H_2^* and H_2^{**}) are shown. Generally, the energies in *h*BN are noticeably lower than those in *c*BN. We conclude that H prefers to reside in *h*BN. This is consistent with experiments involving low H concentrations in *c*BN [20]. The lowest-energy configuration in *c*BN is an H interstitial at the bond center, shown in Fig. 1(b). In this configuration, the inserted B–N bond is 52% longer than the normal one. So, the formation energy of this interstitial is quite high even under B-rich condition. We also studied H_2 molecules and H_2^* complexes according to the similar forms in silicon [21]. Like H_2 in silicon, H_2 favors the tetrahedral interstitial site (T_d) in *c*BN, see Fig. 1(b). But the bond length of H_2 is compressed from 0.76 Å (for free molecule) to 0.71 Å. Another interesting complex named H_2^* has one H at bond center and the other at the B antibonding site, see Fig. 1(b). But these two kinds of double H defects hold large formation energies (>7.22 eV for the H_2 and >6.47 eV for H_2^*). In other words, H is unlikely to be present in a substantial amount in *c*BN.

Compared to *c*BN, the formation energy of an H interstitial in *h*BN is much lower—i.e., 2.25 eV under B-rich condition. This is because no B–N bond is broken to produce an interstitial, see Fig. 1(c). Like H on graphene, an H interstitial in *h*BN tends to bond with B and then make the plane slightly bulged out (by ~0.1 Å). In *h*BN, the most stable form is an H_2 molecule (0.95 eV at B-rich condition), due to a large space for the insertion in Fig. 1(c). The H_2 stays at the center of a honeycomb parallel to the BN layer. Considering an unchanged bond length, this H_2 should hold the similar character as the free H_2 does. In terms of energy, another possible existing defect named H_2^{**} has one H connecting to B and the other connecting to neighboring N shown in Fig. 1(c). Clearly, these attached B and N atoms are in sp^3-bonding configuration. Therefore, it seems that H can aid the growth of *c*BN. However, an H atom prefers to have a single bond and finally limits the extension of the sp^3 framework.

Generally, various H-containing compounds are used as precursors in the CVD growth, so H is found in high concentration (>1%) in *h*BN [12]. However, the present formation energy (~1.0 eV for H_2 and ~1.6 eV for H_2^{**}) indicates it barely reaches such high concentration. For example, assuming a 500 °C growth temperature, the formation energy must be as low as 0.3 eV for a percent level incorporation in *h*BN. In fact, we note that infrared spectroscopy (IR) has observed vibration modes related to H–N and H–B bonds [22]. That raises an interesting question: can high-concentration H defects be more stable than the isolated one? We calculated the formation energy of H_2 and H_2^{**} with increasing concentration. The results are shown in Fig. 2. Here, the concentration is defined as the occupation percentage of available sites between two BN layers for H_2 and the coverage percentage on one BN plane for H_2^{**}. The averaged energy of H_2 decreases from ~1.0 eV at low concentration to 0.22 eV at 100% occupation. For H_2^{**}, the energy decreases from ~1.6 eV at low concentration to 0.20 eV at 100% occupation. As seen in Fig. 2 inset, the full covered BN plane by H_2^{**} is changed to a *zigzag*-like structure and results in lowering total energy. These results very clearly suggest that H_2 or H_2^{**} can automatically gather to form clusters in *h*BN. This low energy is consistent with a substantial amount of H in *h*BN in experiments [12,22].

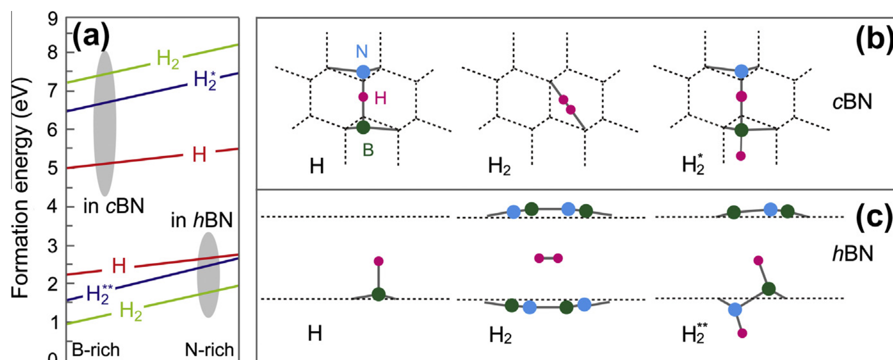

Fig. 1. (a) Formation energies of H defects as function of growth condition. (b) Schematic drawings of various H defects in *c*BN. (c) Same as (b) but for *h*BN. The perfect lattice grid is represented by dashed lines, while the H atoms as well as the B and N atoms that undergo significant relaxations are represented by spheres, as labeled in *c*BN.

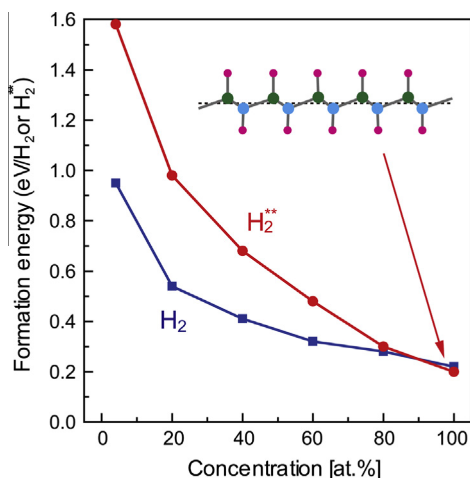

Fig. 2. Formation energies of H_2 and H_2^{**} (per 2H) in *h*BN as function of H concentration. The concentration is defined as the filling percentage of the hexagon-center sites between two BN planes for H_2 and the coverage percentage of one BN plane for H_2^{**}. The inset shows a BN plane fully covered by H_2^{**}, where the color scheme is the same as in Fig. 1.

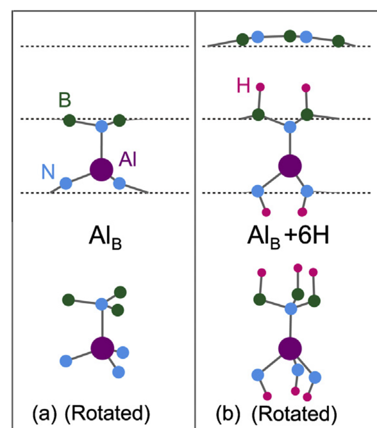

Fig. 3. Schematic drawings of the Al_B defect (a) and the Al_B-6H complex (b) in *h*BN. The upper part shows side views of the defects parallel to the BN planes, represented by dashed lines, while the lower part shows slightly rotated views. Al atoms are represented by large purple spheres, while the color scheme for other atoms is the same as in Fig. 1.

3.2. Vibration frequency

In order to further identify the IR frequency, the stretch-mode vibration of H_2 and H_2^{**} in *h*BN were analyzed by tracing the potential energy of the vibration by H displacement [23]. Here, the displacement of the B or N in the *h*BN can be neglected because H is obviously lighter. The reduced mass of the oscillator is used. We included the anharmonic effect. The results are shown in Table 1. To test the reliability, we also calculated the stretch frequency of free H_2 in a vacuum. The calculated 3849 cm^{-1} is somewhat lower than the measured 4200 or 4161 cm^{-1} in experiments [24] or [25], but is fairly consistent with the previous theoretical work [26]. Here, the calculated H-H stretch frequency of H_2 in *h*BN is 3802 cm^{-1}. In *h*BN experiment, a vibration mode of 4000 cm^{-1}, which is smaller than the experimental frequency of the free H_2, was observed [22]. Therefore, we assign this mode to the interstitial H_2 in *h*BN. For the H_2^{**}, the calculated frequencies related to H–B and H–N bonds are 2435 cm^{-1} and 2971 cm^{-1}. Considering the systematic underestimation in our calculation, we correlate them to the experimental vibration modes of 2550 cm^{-1} and 3200 cm^{-1} [22] or 2500 cm^{-1} and 3300 cm^{-1} [27] in *h*BN. Therefore, the present proposed H_2 and H_2^{**} models actually exist in experiment.

3.3. Binding with Al

In fact, intentional doping has also been tried to control the growth or improve the performance of BN. For example, due to the fourfold coordination of AlN, Al in *h*BN can potentially serve as a nucleus, aiding the transition from *h*BN to *c*BN [28]. However, recent experiment [29] showed that there was no significant improvement on the growth of *c*BN from *h*BN when Al was doped. Here, we analyze the interaction between Al and H in *h*BN to understand such observation. In Fig. 3(a), the stable Al tends to replace B and also move away from the BN plane while bonding to N in the upper plane. This fourfold Al_B structure is actually a nucleus of cubic phase. Yet, further calculations show H tends to bind with B and N close to Al_B. See Fig. 3(b), up to 6 H can be attached around Al_B. To evaluate the energy cost for adding H to Al_B, we employed Eq. (1) but changed the total energy of bulk *h*BN to that including Al_B. The energy for the two H (one attached to B and the other to N) is just 0.78 eV. This indicates they readily form once Al has been incorporated in *h*BN. The average energy cost for 6 H to Al_B is still not high, 1.37 eV/2H. We notice that these H also realize sp^3-like configuration around Al. But such sp^3 network still cannot be extended due to single bond character of H. Therefore, under H ambient, these Al_B nucleuses are all passivated, explaining the experiment above. The present Al_B and multi-H model is also supported by that increment of H induced by Al is about three times of that of Al [29].

Table 1
Our calculated frequencies of H-related defects in *h*BN. The frequencies were calculated by considering both harmonic and anharmonic contributions. Experimental results are also listed for comparison.

Bond	Calculation (cm^{-1})	Experiment (cm^{-1})
H–H (of H_2 in vacuum)	3849	4200 [24], 4161 [25]
H–H (of H_2 in *h*BN)	3802	4000 [22]
H–B (of H_2^{**} in *h*BN)	2435	2550 [22], 2500 [27]
H–N (of H_2^{**} in *h*BN)	2971	3200 [22], 3300 [27]

4. Conclusion

In conclusion, we systemically studied the thermodynamic and vibration properties of H in BN crystal using first-principles calculation. Essentially, H prefers to reside in *h*BN with forms of H_2 and H_2^{**} rather than in *c*BN. Unexpectedly, these H_2 and H_2^{**} can automatically gather to form clusters. In the presence of H, the *c*BN phase tends to be suppressed. Therefore, Al-induced *sp*^{3} nucleus in *h*BN is readily passivated. That explains why Al offers no significant improvement to grow *c*BN from *h*BN. The present study offers an atomic picture to control the phase stability and quality of BN related materials through careful H selection.

Acknowledgements

This work was supported by NSFC (Nos. 11104109, 61077026 and 60976037), U.S. DOE Office of Basic Energy Sciences (No. DE-SC0002623), and NANOTEC, NSTDA (Thailand) through its Center of Excellence Network program. We thank the Computational Center for Nanotechnology Innovations at RPI and the High Performance Computing Center at JLU.

References

[1] O. Mishima, J. Tanaka, S. Yamaoka, O. Fukunaga, Science 238 (1987) 181–183.
[2] K. Watanabe, T. Taniguchi, H. Kanda, Nat. Mater. 3 (2004) 404–409.
[3] C.B. Samantaray, R.N. Singh, Int. Mater. Rev. 50 (2005) 313–344.
[4] Y. Kubota, K. Watanabe, O. Tsuda, T. Taniguchi, Science 317 (2007) 932–934.
[5] P.B. Mirkarimi, K.F. McCarty, D.L. Medlin, Mater. Sci. Eng. Rep. 21 (1997) 47–100.
[6] C. Ronning, E. Dreher, H. Feldermann, M. Gross, M. Sebastian, H. Hofsäss, Diamond Relat. Mater. 6 (1997) 1129–1134.
[7] G. Chen, X. Zhang, B. Wang, X. Song, B. Cui, H. Yan, Appl. Phys. Lett. 75 (1999) 10–12.
[8] M. Mieno, T. Yoshida, Jpn. J. Appl. Phys. 29 (1990) L1175.
[9] H. Saitoh, W.A. Yarbrough, Appl. Phys. Lett. 58 (1991) 2482–2484.
[10] D.J. Kester, R. Messier, J. Appl. Phys. 72 (1992) 504–513.
[11] W.J. Zhang, Y.M. Chong, I. Bello, S.T. Lee, J. Phys. D: Appl. Phys. 40 (2007) 6159.
[12] R. Freudenstein, S. Reinke, W. Kulisch, Surf. Coat. Technol. 97 (1997) 270–274.
[13] R.Q. Zhang, T.S. Chu, C.S. Lee, S.T. Lee, J. Phys. Chem. B 104 (2000) 6761–6766.
[14] K.P. Loh, M. Nishitani-Gamo, I. Sakaguchi, T. Taniguchi, T. Ando, Diamond Relat. Mater. 8 (1999) 1296–1300.
[15] D.M. Ceperley, B.J. Alder, Phys. Rev. Lett. 45 (1980) 566–569.
[16] G. Kresse, D. Joubert, Phys. Rev. B 59 (1999) 1758–1775.
[17] G. Kresse, J. Furthmüller, Comput. Mater. Sci. 6 (1996) 15–50.
[18] R.W.G. Wyckoff, Crystal Structure, second ed., Interscience, New York, 1963.
[19] S.B. Zhang, J.E. Northrup, Phys. Rev. Lett. 67 (1991) 2339–2342.
[20] M. Kuhr, R. Freudenstein, S. Reinke, W. Kulisch, G. Dollinger, A. Bergmaier, Diamond Relat. Mater. 5 (1996) 984–989.
[21] S.B. Zhang, W.B. Jackson, Phys. Rev. B 43 (1991) 12142–12145.
[22] W.J. Zhang, S. Matsumoto, Chem. Phys. Lett. 330 (2000) 243–248.
[23] S. Limpijumnong, S.B. Zhang, Appl. Phys. Lett. 86 (2005) 151910–151913.
[24] M.I. Eremets, I.A. Troyan, Nat. Mater. 10 (2011) 927–931.
[25] B.P. Stoicheff, Can. J. Phys. 35 (1957) 730–741.
[26] S. Limpijumnong, MRS Proc. 813 (2004) H3.6.
[27] H. Saitoh, W.A. Yarbrough, Appl. Phys. Lett. 58 (1991) 2228–2230.
[28] A. Kolitsch, X. Wang, D. Manova, W. Fukarek, W. Möller, S. Oswald, Diamond Relat. Mater. 8 (1999) 386–390.
[29] T. Pfeifer, F. Richter, T. Welzel, H. Kupfer, P. Willich, J. Appl. Phys. 93 (2003) 2009–2014.